Inorg. Chem. **2006**, *45*, 2718–2726

$Cu_4Mo_6Se_8$: Synthesis, Crystal Structure, and Electronic Structure of a New Chevrel Phase Structure Type

Michael A. McGuire,[†] Chinmoy Ranjan,[‡] and Francis J. DiSalvo*[,‡]

Department of Physics, Clark Hall, Cornell University, Ithaca, New York 14853, Department of Chemistry and Chemical Biology, Baker Laboratory, Cornell University, Ithaca, New York 14853

Received November 21, 2005

$Cu_4Mo_6Se_8$ has been synthesized by intercalation of Cu into $Cu_2Mo_6Se_8$ at room temperature, and its crystal structure has been determined. This compound crystallizes in the triclinic space group $P\bar{1}$, with $a = 6.7609(8)$ Å, $b = 6.8122(7)$ Å, $c = 7.9355(10)$ Å, $\alpha = 70.739(4)°$, $\beta = 72.669(4)°$, $\gamma = 84.555(5)°$, and $Z = 1$. Instead of residing in the voids between corners or edges of Mo_6Se_8 clusters as in the classic $R\bar{3}$ Chevrel structure, the Cu atoms in $Cu_4Mo_6Se_8$ fully occupy four sites between faces of two adjacent Mo_6Se_8 clusters. Thus, two of the six Mo atoms in each cluster do not have capping Se atoms from neighboring clusters. This represents a new triclinic structure type for Chevrel phases. In addition to the synthesis and crystal structure, we present and discuss results from electronic structure calculations using both extended Hückel and density functional theory. These calculations predict $Cu_4Mo_6Se_8$ to be metallic. We also report results from Cu intercalation into Chevrel phase sulfides and tellurides. Preliminary experiments suggest that a telluride analogue of $Cu_4Mo_6Se_8$ exists.

Introduction

Chevrel phase materials have been known since 1971[1] and have been extensively studied as superconductors[2] and more recently as thermoelectric materials.[3−5] These compounds contain octahedral clusters of six Mo atoms, with eight face-capping chalcogen atoms, Q. Chevrel phases are known for Q = S, Se, and Te, but in this paper, we will restrict our discussion primarily to Chevrel phase selenides. In the classic Chevrel phases (space group $R\bar{3}$), each unit cell contains one pseudo-cubic Mo_6Se_8 cluster.[1] The clusters are rotated by about 26° about the 3-fold axis, which allows the Mo atoms on each face of each cluster to be capped by a Se atom at the corner of a cluster in a neighboring unit cell. Thus, each Mo atom is in square pyramidal coordination to five Se atoms. The resulting 3-D framework has channels made up of interconnected cavities which can be filled with a wide variety of guest atoms.[2] The electronic structure of such materials can be described in a rigid-band framework with the guest atoms "donating" their valence electrons to (potentially) fill the conduction bands of Mo_6Se_8 which arise primarily from Mo d orbitals. In some cases, the filling causes a slight distortion of the crystal structure, lowering the symmetry of the lattice from rhombohedral to triclinic (space group $P\bar{1}$).[2] In addition, aliovalent substitutions can be made on the Mo atom and the Se atom sites in the Mo_6Se_8 cluster.[6,7] These fillings and substitutions offer means of tuning the electronic properties of Chevrel phase compounds.

Due to their versatile compositions and interesting electronic properties, these compounds have attracted considerable attention, as noted above. Most Chevrel phase research has been focused on superconductivity, since these materials have very high critical fields.[2] However, interest in Chevrel-phase materials for thermoelectric applications recently has increased.[3] Thermoelectric generators convert heat flow into electrical currents and are used, for example, to power space probes which are too far from the sun to use solar energy.[8] It is known that good thermoelectric materials should be

* To whom correspondence should be addressed. E-mail: fjd3@cornell.edu.
[†] Department of Physics, Cornell University.
[‡] Department of Chemistry and Chemical Biology, Cornell University.

(1) Chevrel, R.; Sergent, M.; Prigent, J. *J. Solid State Chem.* **1971**, *3*, 315.
(2) *Topics in Current Physics: Superconductivity in Ternary Compounds I*; Fischer, O., Maple, M. B., Eds.; Springer-Verlag: Berlin, 1982.
(3) Caillat, T.; Fleurial, J.-P. *J. Phys. Chem. Solids* **1998**, *59*, 1139.
(4) Caillat, T.; Fleurial, J.-P.; Snyder, G. J. *Solid State Sciences* **1999**, *1*, 535.
(5) Roche, C.; Pecheur, P.; Toussaint, G.; Jenny, A.; Scherrer, H.; Scherrer, S. *J. Phys.: Condens. Matter* **1998**, *10*, L333.
(6) Perrin, A.; Sergent, M.; Fischer, O. *Mater. Res. Bull.* **1978**, *13*, 259.
(7) Perrin, A.; Chevrel, R.; Sergent, M.; Fischer, O. *J. Solid State Chem.* **1980**, *33*, 43.
(8) Heikes, R. R.; Ure, R. W., Jr. *Thermoelectricity: Science and Engineering*; Interscience Publishers: New York, London, 1961.

10.1021/ic052013p CCC: $33.50
Published on Web 02/11/2006

semiconductors with low lattice thermal conductivity.[8] The disorder induced by substitution and partial filling of Chevrel phases has been shown to significantly decrease their thermal conductivity.[4] These fillings and cluster core substitutions can also be used to tune the electronic properties from metallic to semiconducting, as discussed below.

The unfilled Chevrel phase Mo_6Se_8 is metallic. However, band-structure calculations on the extended structure,[5,9] as well as molecular orbital (MO) calculations on the Mo_6Se_8 unit[10] (vide infra), show that it can be made semiconducting by the addition of four electrons per cluster (or unit cell). By adding four (or nearly four) electrons per unit cell, using filling or substitutions, semiconducting Chevrel phases have been realized in several cases. These include the selenides $Ti_{0.88}Mo_6Se_8$,[4] $Mo_4Ru_2Se_8$,[7] and $Mo_2Re_4Se_8$.[3]

One interesting case in which a semiconducting compound has not been attained is the copper-filled Chevrel phase selenides. Although not semiconducting, the copper-filled compound $Cu_{3.1}Mo_6Se_8$ shows the best thermoelectric performance at high temperature of any Chevrel phase studied to date.[4] Efforts to improve this material by increasing the Cu concentration have not been successful. This is not true for the sulfides, and $Cu_4Mo_6S_8$ has been synthesized by the electrochemical intercalation of Cu.[11] One reason for the limited Cu content seen in the Se compounds may be the high temperatures (>1100 °C) at which these materials are typically prepared. This led us to investigate lower-temperature routes toward Cu-filled Mo_6Se_8.

There have been numerous investigations of the addition of guest atoms to these materials near room temperature. Electrochemical cells have been used to intercalate Li, Mg, Na, Zn, Cd, and Cu into Chevrel phase sulfides and selenides.[12] One study by Selwyn and McKinnon investigated the intercalation of Li into already partially filled $Cu_yMo_6Se_8$ ($0 < y < 2.5$).[13] They found, in addition to a series of Li/Cu-filled phases, an unidentified Cu-rich phase. They also showed that this phase could be produced by the intercalation of Cu into $Cu_yMo_6Se_8$, proving that no Li was incorporated into the structure. The authors were unable to prepare the copper-rich compound as a single phase ($Cu_{1.7}Mo_6Se_8$ was always present as an impurity), and were unable to index the observed powder X-ray diffraction peaks. In this paper, we report the crystal structure of this copper-rich Chevrel phase.

Unlike many previous authors' work, our low-temperature studies were not performed in an electrochemical cell but in a specially designed apparatus described below. We characterized the products of our reactions using powder X-ray diffraction, quantitative electron microprobe analysis, and single-crystal X-ray diffraction. We determined the composition of this phase to be $Cu_4Mo_6Se_8$. This compound adopts a new structure type and represents the first example of an extended structure with Chevrel-like Mo_6Se_8 layers that are not joined to each other through Mo−Se bonding. The only interlayer connections are through Cu−Se bonding. This results in two Mo atoms on each cluster having square-planar Se coordination, while the other four have the usual square pyramidal coordination. In addition to the synthesis and crystal structure of $Cu_4Mo_6Se_8$, we discuss the electronic consequences of the separation of the Mo_6Se_8 layers.

Experimental Section

Synthesis. Mo_6S_8 and Mo_6Se_8 cannot be prepared directly from the elements,[14] so the starting materials used in our intercalation studies for the sulfide and selenide systems were $Cu_2Mo_6Q_8$ (Q = S, Se). For the telluride system, Mo_6Te_8 was used since it can be produced by direct reaction of Mo and Te. These compounds were synthesized from the elements: Cu (Fisher, electrolytic powder), Mo (Aldrich, 99.9%, −100 mesh), S (Cominco, 99.99%), Se (unspecified source, 99.999%), and Te (Johnson Matthey, 99.9999%). The Mo (Cu) powder was reduced in forming gas at 1000 °C (300 °C) for about 24 (3) h and subsequently stored and handled inside an argon-filled glovebox. The S, Se, and Te were used as received. Stoichiometric mixtures (typically 2−3 g total) were sealed in evacuated silica tubes and heated over 1 day to 400 °C and held at this temperature for 1 day. The tubes were then shaken to mix the reaction products but not opened. The tubes were then heated to various temperatures, from 900 to 1200 °C, held there for 3 days, and then cooled naturally to room temperature with the furnace power off. The resulting powdered products were almost single-phase $Cu_2Mo_6Q_8$ or Mo_6Te_8 with lattice constants matching closely those reported in the literature.[2] A small amount (~5%) of MoQ_2 impurity was present in some samples.

It is common to prepare partially Cu-filled Chevrel phases and then remove the Cu to obtain unfilled Mo_6Q_8, which cannot be prepared from the elements for Q = S, Se, as noted above.[14] One way in which this is done is through reaction with iodine dissolved in acetonitrile (AN).[15] The Chevrel phase is oxidized by the I_2 in solution and forms CuI, which is soluble in AN (3.4 wt%[16]).

As a means for adding Cu to the Chevrel phase, we essentially performed this reaction in reverse. Copper was intercalated through CuI dissolved in AN from an excess supply of elemental Cu in electrical contact with the Chevrel phase. In the presence of excess Cu, this reaction should proceed until it is no longer energetically favorable to add more Cu to the Chevrel phase (assuming that the diffusion rate of Cu in the Chevrel phase remains large enough). A special device was constructed for this reaction, designed to ensure the required electrical contact between the Cu reservoir and the sample.

Our Cu intercalation apparatus is shown in Figure 1. It consists of a glass tube which is threaded on one end and sealed with a flat glass plate on the other. The glass plate is held in place with Torr-Seal epoxy. The sample (typically 200−500 mg) is placed between two accurately weighed cylindrical copper blocks, machined from

(9) Roche, C.; Chevrel, R.; Jenny, A.; Pecheur, P.; Scherrer, H.; Scherrer, S. *Phys. Rev. B* **1999**, *60* 16442.
(10) Hughbanks, T.; Hoffmann, R. *J. Am. Chem. Soc.* **1983**, *105*, 1150.
(11) Fischer, C.; Gocke, E.; Stege, U.; Schöllhorn, R. *J. Solid State Chem.* **1993**, *102*, 54.
(12) Dahn, J. R.; McKinnon, W. R.; Coleman, S. T. *Phys. Rev. B* **1985**, *31*, 484. Levi, M. D.; Gizbar, H.; Lancry, E.; Gofer, Y.; Levi, E.; Aurbach, D. *J. Electroanal. Chem.* **2004**, *569*, 211. Gocke, E.; Schramm, W.; Dolscheid, P.; Schoellhorn, R. *J. Solid State Chem.* **1987**, *70*, 71.
(13) Selwyn, L. S.; McKinnon, W. R. *J. Phys. C: Solid State Phys.* **1988**, *21*, 1905.
(14) Belin, S.; Chevrel, R.; Sergent, M. *J. Solid State Chem.* **1999**, *145*, 159.
(15) Tarascon, J. M.; Waszczak, J. V.; Hull, G. W., Jr.; DiSalvo, F. J.; Blitzer, L. D. *Solid State Comm.* **1983**, *47*, 973.
(16) Janz, G. J.; Tomkins, R. P. T. *Nonaqueous Electrolytes Handbook II*; Academic Press: New York, 1973.

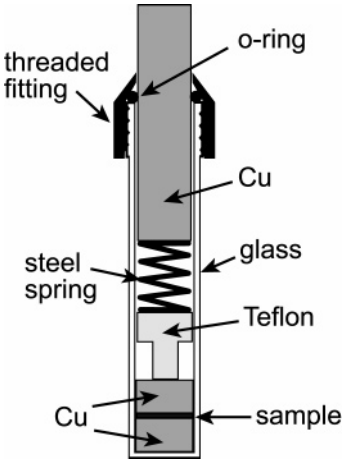

Figure 1. Drawing of the apparatus used for the room-temperature intercalation studies. The outer diameter of the glass tube is approximately 19 mm.

an oxygen-free high-conductivity copper rod to fit snugly inside the glass tube, in the bottom of the apparatus. The faces of the copper blocks are cleaned with 1200 grit SiC paper before each run. A solution of CuI in AN (about 2 wt%) is added so that the sample and Cu blocks are immersed. A copper rod and steel spring are used to apply pressure to the sample, ensuring good electrical contact between the powder grains and the copper, and the O-ring seal is tightened to maintain the pressure. A Teflon spacer is used to keep the steel spring out of the CuI/AN solution.

The intercalation experiments were carried out inside an argon-filled glovebox. The reactions were allowed to proceed for various lengths of time, from 2 h up to 10 days. The apparatus was then removed from the glovebox and opened. The product was removed, filtered, and rinsed with AN in air.

Characterization. Powder X-ray diffraction (PXRD) patterns were collected on a Scintag 2000 theta-theta diffractometer using Cu Kα radiation. Quantitative electron microprobe analysis was performed using a JEOL 8900R electron microprobe operating at 15 kV and approximately 20 nA. Measurements were carried out in wavelength dispersive mode, using pure elemental Cu, Mo, and Se as standards. The powdered samples were embedded in electrically conducting epoxy mounts and then polished using 1200 grit SiC paper followed by a 1 μm diamond suspension on a Struers Rotopol/Rotoforce polishing system. The samples and standards were coated with approximately 250 Å of carbon prior to analysis. Single-crystal X-ray diffraction data were collected on a Bruker APEX diffractometer. The data were collected using the program SMART and integrated with SAINT-*Plus*.[17] Absorption corrections and space group determinations were performed using SADABS[18] and XPREP,[19] respectively. SHELXS and SHELXL were used for the crystal structure solution (direct methods) and refinement (full-matrix least-squares on F^2) within the WinGX program suite.[20] Scattering factors for all atoms were taken from the International Tables Vol. C, Tables 4.2.6.8 and 6.1.1.4. Magnetic susceptibility measurements were performed using a Quantum Design MPMS.

(17) *APEX2 (Version 1.22, 2004) and SAINT-Plus (Version 7.06a, 2003)*; Bruker Analytical X-ray Instruments, Inc.: Madison, WI.
(18) Sheldrick, G. M. *SADABS (Version 2.10) program for absorption correction*; Bruker Analytical X-ray Instruments, Inc., Madison, WI, 2003.
(19) *XPREP program for determination of space groups*; Bruker Analytical X-ray Instruments, Inc., Madison, WI, 2003.
(20) Farrugia, L. *J. Appl. Crystallogr.* **1999**, *32*, 837.

Calculations

Extended Hückel molecular orbital and electronic band-structure calculations were carried out using YAeHMOP.[21] The default parameters were used for all orbitals in the calculations and can be found in the footnotes.[22]

GGA-PW91[23,24] DFT-based periodic calculations were carried out in a PAW[25,26] basis using the VASP[27] package. The plane wave cut-off energy was fixed at 500 eV. A $6 \times 6 \times 6$ Monkhorst Pack[28] grid of K points was used. The optimized geometry used to calculate the band structure and density of states varied less than 3% from the experimental values (optimized lattice parameters: $a = 6.89$ Å, $b = 6.92$ Å, $c = 8.03$ Å, $\alpha = 71.52°$, $\beta = 72.64°$, $\gamma = 84.83°$). The Wigner Seitz radii used to calculate projected densities of states were 1.455 Å for Mo, 1.312 Å for Cu, and 1.164 Å for Se. All electronic iterations were converged within 10^{-4} eV.

Results of Intercalation Studies

The Chevrel phase sulfide system $Cu_xMo_6S_8$ has been extensively studied. Of particular relevance to the current work are the results from in situ X-ray studies during the formation of these phases via electron/ion transfer.[11] Those authors were able to synthesize samples with $1 \leq x \leq 4$ by electrochemical reactions. Before discussing the selenides, the main focus of our work, we briefly report here the results of the intercalation of the sulfide $Cu_2Mo_6S_8$ in our apparatus.

$Cu_2Mo_6S_8$ was synthesized as described above, with the final heating at 1100 °C. PXRD of the resulting powder showed it to be essentially single-phase, with one small peak attributed to highly oriented MoS_2. The powder pattern was indexed with the program TREOR,[29] which gave a hexagonal unit cell volume of 819.9 Å^3, in good agreement with previous work, which found $V = 818.3$ Å^3 for $x = 1.88$.[11] This material was then intercalated in our apparatus for 1 day and then removed and analyzed by PXRD. This product was then put back into the apparatus and intercalated for one more day. Measurement of the mass loss of the Cu blocks suggested an average stoichiometry of $Cu_{3.6}Mo_6S_8$ after the first intercalation run and $Cu_{3.7}Mo_6S_8$ after the second run. The hexagonal unit cell volume determined by PXRD after the first run was 849.6 Å^3 and after the second run was 850.4 Å^3. These are in good agreement with the previous study, which found $V = 849.9$ Å^3 for $x = 3.6$.[11] This shows that the mass loss of the Cu reservoirs is a reliable way to determine the final stoichiometry of the intercalated compound. The same authors found that the maximum Cu

(21) Landrum, G. *YAeHMOP (Version 3.0)*, http://yaehmop.sourceforge.net.
(22) Extended Hückel parameters, H_{ii} (eV) and ζ for s and p states, H_{ii} (eV), ζ_1, c_1, ζ_2, c_2 for d states: Mo 5s, −8.34, 1.96; Mo 5p, −5.24, 1.9; Mo 4d, −10.5, 0.5899, 4.54, 0.5899, 1.9; Cu 4s, −11.4, 2.2; Cu 4p, −6.06, 2.2; Cu 3d, −14.0, 0.5933, 5.95, 0.5744, 2.3; Se 4s, −20.5, 2.44; Se 4p −14.4, 2.07.
(23) Perdew, J. P.; et al. *Phys. Rev. B* **1992**, *46*, 6671.
(24) Perdew, J. P.; et al. *Phys. Rev. B* **1993**, *48*, 4978.
(25) Blöchl, P. E. *Phys. Rev. B* **1994**, *50*, 17953.
(26) Kresse, G.; Joubert, D. *Phys. Rev. B* **1999**, *59*, 1758.
(27) Kresse, G.; Hafner, J. *Phys. Rev. B* **1993**, *47*, 558. Kresse, G.; Hafner, J. *Phys. Rev. B* **1994**, *49*, 14251. Kresse, G.; Furthmüller, J. *Comput. Mater. Sci.* **1996**, *6*, 15. Kresse, G.; Furthmüller, J. *Phys. Rev. B* **1996**, *54*, 11169.
(28) Monkhorst, H. J.; Pack, J. D. *Phys. Rev. B* **1976**, *13*, 5188.
(29) Werner, P.-E.; Eriksson, L.; Westdahl, M. *J. Appl. Crystallogr.* **1985**, *18*, 367.

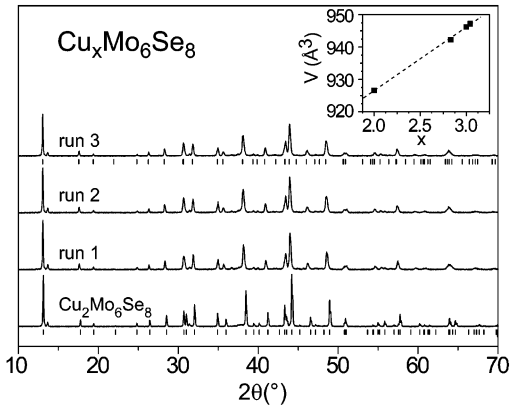

Figure 2. PXRD patterns for products of the intercalation of $Cu_2Mo_6Se_8$ made at 900 °C. Tick marks locate the calculated peak positions for the indexed $R\bar{3}$ Chevrel phase unit cells for the starting material and for the final product. The inset shows the hexagonal unit cell volume versus composition.

content realized by high-temperature reactions with subsequent slow cooling was $x = 3.66$, suggesting that phases prepared at room temperature by electrochemical reaction with $3.66 \leq x \leq 4$ are metastable. Thus, it is not surprising that our intercalation, which should stop at the thermodynamic limit of x, produced $Cu_{3.7}Mo_6S_8$.

Similar results were seen when $Cu_2Mo_6Se_8$, which was synthesized at 900 °C, was intercalated in our apparatus. This material was intercalated for 2.5 days and then analyzed by PXRD. The product was then placed back into the apparatus and further intercalated for 3 days. After analysis of the product of the second run, a third intercalation was performed. The PXRD patterns for the starting material and for the product after each intercalation is shown in Figure 2. The inset shows the indexed unit cell volume versus x determined by mass loss from the Cu blocks. The final product was $Cu_{3.04}Mo_6Se_8$, close to the maximum Cu content ($x = 3.1$) that has been achieved through high-temperature synthesis. [4]

More interesting results were produced when the starting material was synthesized at higher temperature. $Cu_2Mo_6Se_8$ was made as described in the Experimental Section, with the second heating carried out at 1100 °C. This material was then heated for 2 days at 1200 °C in a sealed, evacuated silica tube. The behavior of the resulting material upon intercalation was dramatically different than that described above for $Cu_2Mo_6Se_8$ made at 900 °C. The PXRD patterns of the starting material and the intercalation product are shown in Figure 3. Upon intercalation, a second phase is formed but with a significant amount of rhombohedral $Cu_xMo_6Se_8$ still present. It is interesting to note that, upon deintercalation of Cu, the mixed-phase intercalation product is transformed completely into single-phase Mo_6Se_8 (Figure 3). This shows that the transformation between rhombohedral $Cu_xMo_6Se_8$ and the new phase at room temperature is reversible with respect to the addition/removal of Cu. On the basis of the reported Bragg peaks of the Cu-rich phase reported by Selwyn and McKinnon,[13] we believe that this is the same material they first observed. Microprobe analysis of the intercalation product showed that all of the crystallites

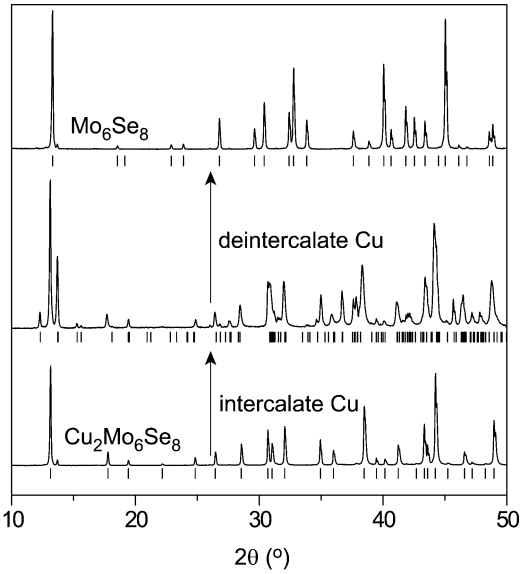

Figure 3. PXRD patterns showing the effect of Cu intercalation into $Cu_2Mo_6Se_8$ which was annealed at 1200 °C and the subsequent deintercalation of Cu from the intercalation product. Tick marks indicate the calculated peak positions for rhombohedral Chevrel phase unit cells in the lower and upper patterns and the new phase $Cu_4Mo_6Se_8$ in the middle pattern.

had the stoichiometry $Cu_xMo_6Se_8$. The average measured Cu content ($x = 3.2$) was close to that determined by the Cu mass loss ($x = 3.1$). However, the grains could be divided in to two groups based on the value of x. One group had $x \approx 2.5$ while the second had $x \approx 4$. Thus, we conclude that the rhombohedral phase is $Cu_{\sim 2.5}Mo_6Se_8$ and the new phase is $Cu_{\sim 4}Mo_6Se_8$.

Repeated intercalations of these two-phase products did not significantly increase the fraction of $Cu_4Mo_6Se_8$, but led only to a gradual increase in the Cu content of the rhombohedral phase. This suggests that only certain crystallites in the starting material are capable of transforming into $Cu_4Mo_6Se_8$. Since this phase only forms from starting materials that have been annealed at higher temperatures, we believe that defects or impurities are important in allowing the transformation to occur. It has been shown that the high-temperature synthesis (~1200 °C) of $Mo_6Se_{8-x}S_x$ can lead to the self-intercalation of Mo into the cavities.[30,31] In addition, several authors have studied the substitution of O for S in Chevrel phase sulfides.[32] In these studies, oxygen was intentionally added to the starting mixture in the form of binary metal oxides. X-ray and neutron diffraction structure refinements indicated that the products had compositions near $M_xMo_6Se_{7.8}O_{0.2}$, with M = Cu, Sn, and Pb. However, even with oxygen-free starting materials, it is possible that some oxygen may enter the samples via the low-pressure gaseous species SiO and O_2 present inside the silica tubes at high temperatures. Partial pressures of SiO and O_2 over silica near 1200 °C are expected to be on the order of 10^{-6} Torr.[33] We have also observed the formation of significant amounts of triclinic $Cu_4Mo_6Se_8$ from the

(30) See ref 14.
(31) Belin, S.; Burel, L.; Chevrel, R.; Sergent, M. *Mater. Res. Bull.* **2000**, *35*, 151.

reaction of 4Cu + 6Mo + 8Se at 1100 °C when the starting materials (Cu and Mo) were not first reduced in forming gas. The same reaction using reduced metals showed no evidence of the triclinic phase. This supports the hypothesis that the presence of defects or impurities is important for the formation of $Cu_4Mo_6Se_8$.

Chevrel phase tellurides are not likely to be promising high-temperature thermoelectric materials, partly due to their lower decomposition temperatures. However, we performed preliminary studies of Cu intercalation into Mo_6Te_8, with the aim of determining whether a Te analogue of triclinic $Cu_4Mo_6Se_8$ exists. Our room-temperature intercalation of Mo_6Te_8 (which was made from the elements at 1000 °C) produced a material with average composition $Cu_{1.8}Mo_6Te_8$ which had a powder pattern similar to that seen for the slightly distorted triclinic phases such as $Ti_{0.88}Mo_6Se_8$. However, the PXRD pattern of the product of the reaction 4Cu + Mo_6Te_8 at 400 °C showed evidence of a $Cu_xMo_6Te_8$ phase isostructural to triclinic $Cu_4Mo_6Se_8$.

Before proceeding to discuss the crystal structure and electronic structure of $Cu_4Mo_6Se_8$ in detail, we will note here briefly some observations that we have made about the stability of rhombohedral Cu-filled Chevrel phases. We have found, on the basis of PXRD studies, that when left in air over the course of several months, the unit cell volumes of $Cu_xMo_6Se_8$ samples decrease significantly. We attribute this to loss of Cu from the Chevrel phase structure, probably through reaction with oxygen at the surface of the grains. This reaction, as in removing Cu with I_2 in AN, occurs because of the high diffusion rate of the Cu in the bulk Chevrel phase. In addition, in some cases the PXRD peaks were broadened, with tails extending toward higher angle. For example, on the basis of a comparison of powder patterns, the $Cu_{3.04}Mo_6Se_8$ intercalation product described above transformed into $Cu_{\sim 2}Mo_6Se_8$ over the course of five months. The $Cu_2Mo_6Se_8$ (synthesized at 900 °C) used as a starting material for the intercalations also showed significant peak broadening and shifts toward lower Cu content after storage in air for about six months. However, no change was seen in the sulfide intercalation product $Cu_{3.7}Mo_6S_8$ upon exposure to air for 10 months. Finally, we note that, when a mixed phase intercalation product containing $R\bar{3}$ $Cu_{2.5}Mo_6Se_8$ and P1 $Cu_4Mo_6Se_8$ was left in air for six months, Cu loss from the rhombohedral phase was observed, while the positions and widths of PXRD peaks corresponding to triclinic $Cu_4Mo_6Se_8$ did not perceptibly change. At present, it is not clear why the "stability" of these different compounds is different.

Crystal Structure of $Cu_4Mo_6Se_8$. Small crystallites were extracted from the two-phase intercalation product and used for single-crystal diffraction studies. While the first crystal selected indexed to a rhombohedral unit cell consistent with $Cu_{2.5}Mo_6Se_8$, the second gave a triclinic cell ($R_{int} = 0.0413$) which matched well with the observed PXRD pattern (see Figure 3). The results of the structure refinement from data collected using this crystal are listed in Table 1. In the reported data, all atomic sites are refined fully occupied. When allowed to refine freely, the occupancy of Cu(1) and Cu(2) refine to 0.987(5) and 0.985(5), respectively, giving a stoichiometry of $Cu_{3.94}Mo_6Se_8$. The corresponding *R* values, for $I > 2\sigma(I)$, are R1 = 0.0331 and wR2 = 0.0668, reduced only slightly from the refinement with fully occupied Cu sites which gives R1 = 0.0333 and wR2 = 0.0697. The residual electron density does not suggest the presence of other atoms in this structure. All but one of the first 20 residual peaks are close to other the atoms in the structure ($d < 2$ Å, and for many $d < 1.5$ Å). These peaks are likely due to truncation of the diffraction data at $2\theta = 55.16°$. The remaining residual (2.07 e/Å^3) is at the special position (0, 1/2, 1/2), with Se as a nearest neighbor, at a distance of 2.18 Å. However, when an Mo, Cu, or O atom is placed at this position, the occupancy of the site refines essentially to zero (<0.009).

Table 1. Crystallographic Data for $Cu_4Mo_6Se_8$[a]

temp	175(5) K	
wavelength	0.71073 Å	
space group	$P\bar{1}$ (No. 2)	
unit cell dimensions	$a = 6.7609(8)$ Å	$\alpha = 70.739(4)°$.
	$b = 6.8122(7)$ Å	$\beta = 72.669(4)°$.
	$c = 7.9355(10)$ Å	$\gamma = 84.555(5)°$.
V	329.36(7) Å^3	
Z	1	
fw	1461.5 g/mol	
density (calcd)	7.449 g/cm^3	
absorption coefficient	33.894 mm^{-1}	
R indices [$I > 2\sigma(I)$]	R1 = 0.0333, wR2 = 0.0697	
R indices [all data]	R1 = 0.0575, wR2 = 0.0755	

[a] $R1 = \sum||F_o| - |F_c||/\sum |F_o|$. $wR2 = [\sum(F_o^2 - F_c^2)^2/\sum (w \cdot F_o^2)^2]^{1/2}$. $w = (\sigma^2 \cdot F_o^2 + (aP)^2 + bP)^{-1}$, $P = [F_o^2 + 2F_c^2]/3$.

The structure of this compound will be discussed here in terms of "sheets" of composition Mo_6Se_8 shown in Figure 4 and "columns" of composition $Cu_4Mo_6Se_8$ shown in Figure 5. The sheets consist of pseudo-cubic Mo_6Se_8 units connected by intercluster Mo−Se bonds. These same sheets are seen in the classic $R\bar{3}$ Chevrel phases. However, in the $R\bar{3}$ structures (and the *slightly distorted* $P\bar{1}$ structures), this same connectivity is also present perpendicular to the sheets, giving a 3-D framework of Mo_6Se_8 units connected by intercluster Mo−Se bonds. In $Cu_4Mo_6Se_8$, on the other hand, a different connectivity exists between the sheets, as shown in Figure 5. The clusters are aligned along the *c* axis face to face, with Cu atoms separating the Mo_6Se_8 units in adjacent sheets. Intersheet connections are made solely by Cu−Se interactions.

In $Cu_4Mo_6Se_8$, the Mo(1) atoms which are nearest the Cu atoms are in square planar coordination by Se, while Mo(2) and Mo(3) are in square pyramidal coordination due to the intercluster Mo−Se bonds. We will see below that the square planar coordination of Mo(1), which is not seen in classic Chevrel phase compounds, has important electronic implications. The coordination of the Mo atoms, as well as the Cu atoms which are each coordinated to three Se atoms, is shown in Figure 6a. The $CuSe_3$ units are not planar. The perpen-

(32) See, for example: Hinks, D. G.; Jorgensen, J. D.; Li, H.-C. *Phys. Rev. Lett.* **1983**, *51*, 1911. Cerny, R.; Yvon, K.; Wakihara, M.; Fischer, P. *J. Alloys Compd.* **1994**, *209*, L29. Chang, C. L.; Tao, Y. K.; Swinnea, J. S.; Steinfink, H. *Acta Crystallogr.* **1987**, *C43*, 1461.
(33) See: Schick, H. L. *Chem. Rev.* **1960**, *60*, 331.

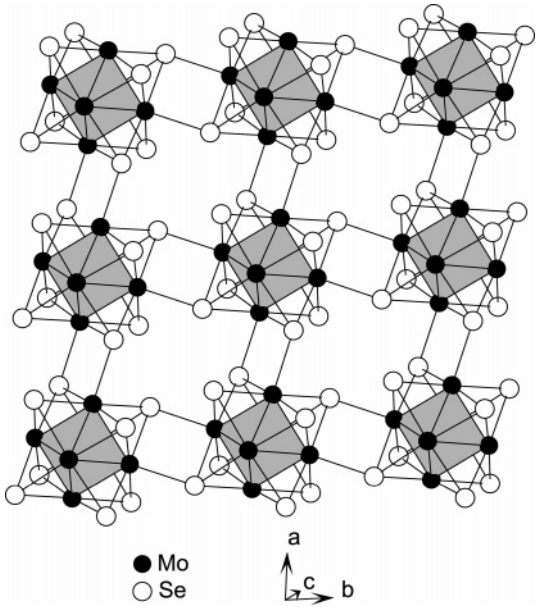

Figure 4. View of the sheets of connected Mo_6Se_8 units found roughly in the *ab* plane of the $Cu_4Mo_6Se_8$ structure.

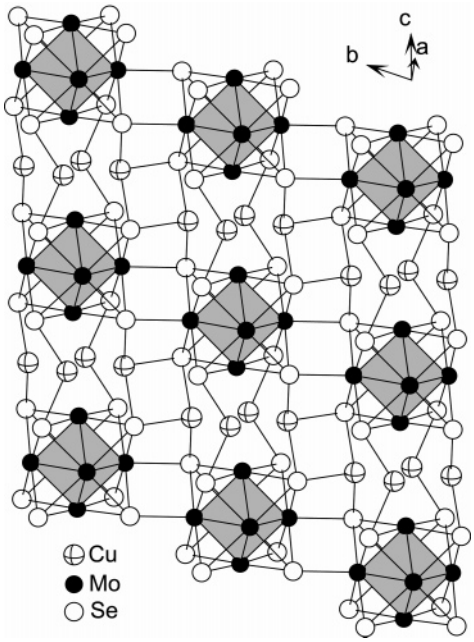

Figure 5. View of the crystal structure of $Cu_4Mo_6Se_8$ showing the connection via Cu atoms of the Mo_6Se_8 sheets shown in Figure 4.

dicular distance between the Cu atom and the plane defined by the three coordinating Se atoms (Figure 6b) is 0.92 and 0.98 Å for Cu(1) and Cu(2), respectively. Linear 2-fold and tetrahedral 4-fold coordination are most common for Cu^{1+}; however, puckered triangular units are also frequently observed (for example, $Tl_2Cu_3Se_2$,[34] $TlCu_7Se_4$,[35] and $CsCu_5S_3$[36]).

Interatomic distances in this compound are reported in Table 2, where the connections between the columns in the structure are marked with asterisks. The Cu−Cu distances are significantly longer than twice the ionic radius for Cu^{1+}

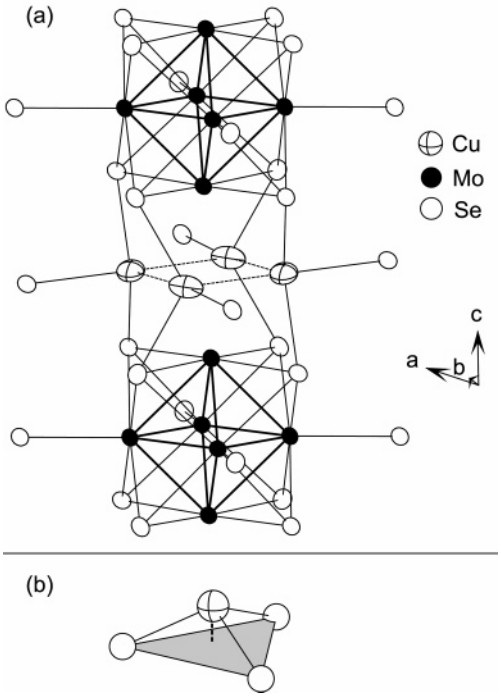

Figure 6. (a) Portion of the $Cu_4Mo_6Se_8$ structure showing the displacement ellipsoids (95% level) for all atoms and the full 3-D coordination of the Cu and Mo atoms. (b) The coordination of Cu by Se, emphasizing the elevation of the Cu atoms (dotted line) above the plane of the coordinating Se atoms.

Table 2. Interatomic Distances (Å) for $Cu_4Mo_6Se_8$[a]

Mo(1)−Mo(2)	2.6958(11), 2.6372(11)
Mo(1)−Mo(3)	2.6555(12), 2.6818(12)
Mo(2)−Mo(3)	2.6814(11), 2.6751(12)
Mo(1)−Se(1)	2.6225(12)
Mo(1)−Se(2)	2.5897(12)
Mo(1)−Se(3)	2.6122(13)
Mo(1)−Se(4)	2.6029(13)
Mo(2)−Se(1)	2.5960(13)
Mo(2)−Se(2)	2.5618(13)
Mo(2)−Se(3)	2.6115(13), 2.6319(12)*
Mo(2)−Se(4)	2.5965(13)
Mo(3)−Se(1)	2.5809(12)
Mo(3)−Se(2)	2.6316(12), 2.6368(13)*
Mo(3)−Se(3)	2.5329(12)
Mo(3)−Se(4)	2.6121(12)
Cu(1)−Se(1)	2.4482(15), 2.6386(17)*
Cu(1)−Se(2)	2.4641(16)
Cu(2)−Se(3)	2.4021(16)
Cu(2)−Se(4)	2.5217(16), 2.6124(15)*
Cu(1)−Cu(2)	2.6718(19), 2.7011(17)
Mo(1)−Cu(1)	2.8013(15), 2.8201(15)
Mo(1)−Cu(2)	2.7478(15), 2.9348(15)

[a] Asterisk denotes intercolumnar connections.

in 4-fold coordination (0.6 Å).[37] The intracolumn Cu−Se distances are similar to those found in Cu_2Se (2.33, 2.47 Å),[38] Cu_3PSe_4 (2.39−2.47 Å),[39] $CuInSe_2$ (2.43 Å),[40] and $Cu_2Mo_6Se_8$ (2.36−2.58 Å)[41], while the intercolumn distances are slightly longer. The Mo−Mo and Mo−Se distances in Table 2 are similar to those found in Mo_6Se_8 in which the Mo−Mo distances are 2.69−2.84 Å, the intracluster Mo−Se

(34) Berger, R.; Erikson L. *J. Less-Common Met.* **1990**, *161*, 101.
(35) Eriksson, L.; Werner, P.-E.; Berger, R.; Meerschaut, A. *J. Solid State Chem.* **1991**, *90*, 61.
(36) Hunter, J.; Bronger, W., *Z. Anorg. Allg. Chem.* **2001**, *627*, 1395.
(37) Shannon, R. D. *Acta Crystallogr. A* **1974**, *32*, 751.
(38) Yamamoto, K.; Kashida, S. *J. Solid State Chem.* **1991**, *93*, 202.
(39) Garin, J.; Parthe, E. *Acta Crystallogr. B* **1972**, *28*, 3672.
(40) Knight, K. S. *Mater. Res. Bull.* **1992**, *27*, 161.

Table 3. Continuous Shape Measures *S* for the Molybdenum Octahedra in $Cu_4Mo_6Se_8$, All $M_xMo_6Se_8$ Chevrel Phases Listed in the Current Version of the ICSD, and the Series $Cu_xMo_6S_8$

composition	S	composition	S
$Cu_4Mo_6Se_8$	0.01117	$La_{0.88}Mo_6Se_8$	0.01406
Mo_6Se_8	0.15117	$La_{0.94}Mo_6Se_8$	0.01198
$Li_{3.2}Mo_6Se_8$	0.00000	$Ce_{0.82}Mo_6Se_8$	0.01473
$PbMo_6Se_8$	0.01030	$Ce_{0.92}Mo_6Se_8$	0.01182
$InMo_6Se_8$	0.01110	$Pr_{0.86}Mo_6Se_8$	0.01485
$Ti_{0.88}Mo_6Se_8$	0.05207*	$Nd_{0.85}Mo_6Se_8$	0.01737
$FeMo_6Se_8$	0.05226*	$Sm_{0.87}Mo_6Se_8$	0.01812
$Co_{0.54}Mo_6Se_8$	0.05752	$U_{0.8}Mo_6Se_8$	0.02105
$Ni_{0.33}Mo_6Se_8$	0.11923*	$Cu_{1.8}Mo_6S_8$	0.03343
$Ni_{1.25}Mo_6Se_8$	0.07502	$Cu_{2.768}Mo_6S_8$	0.00985
$La_{0.82}Mo_6Se_8$	0.01406	$Cu_{2.94}Mo_6S_8$	0.00742
$La_{0.84}Mo_6Se_8$	0.01520	$Cu_{3.66}Mo_6S_8$	0.00377

[a] Asterisk denotes distorted, triclinic structures.

distances are 2.55−2.59 Å, and the intercluster Mo−Se distance is 2.60 Å.[42] In $Cu_4Mo_6Se_8$, the distances among the five-coordinate Mo(2) and Mo(3) atoms are not seen to be significantly different than the distances between Mo(2)/Mo(3) and the four-coordinate Mo(1) atom. It does not seem that the difference in coordination significantly distorts the Mo octahedron. In fact, inspection of the distances in Table 2 shows that the Mo_6 octahedra in $Cu_4Mo_6Se_8$ are quite regular.

A more quantitative measure of the distortion can be gained by comparison of continuous shape measures for the Mo_6 clusters in $Cu_4Mo_6Se_8$ and in other Chevrel phases with known crystal structures.[43] The continuous shape measure, *S*, is a measure of the minimum distance needed to move the vertices of a distorted polyhedron to match a given reference shape. Values of *S*, obtained by comparing the Mo_6 clusters found in $Cu_4Mo_6Se_8$ and all $M_xMo_6Se_8$ Chevrel phases listed in the current version of the Inorganic Crystal Structure Database (ICSD) to a perfect octahedron, are listed in Table 3. These calculations were performed using the program SHAPE.[44] For a perfect, octahedral cluster, $S = 0$. It is interesting to note that $Li_{3.2}Mo_6Se_8$ has $S = 0$. Table 3 shows that the Mo_6 cluster in $Cu_4Mo_6Se_8$ is more regular than those found in unfilled Mo_6Se_8 and in filled Chevrel phases which undergo triclinic distortions. In fact, it is among the least distorted Mo_6 clusters found in the listed selenide Chevrel phases.

Also shown in Table 3 are the calculated *S* values for the sulfide series $Cu_xMo_6S_8$. Inspection of these data show a smooth decrease in *S* from Mo_6Se_8 to $Cu_{3.66}Mo_6Se_8$. As *x* increases, the Mo_6 octahedra become more regular. This is a result of filling Mo−Mo intracluster bonding orbitals by valence electrons donated by Cu (vide infra). For $x \geq 2.76$ in the sulfide series, the Mo_6 octahedra are more regular than that found in triclinic $Cu_4Mo_6Se_8$. This must be attributed, at least in part, to the different coordination environment of Mo(1) and the lower symmetry ($P\bar{1}$) in $Cu_4Mo_6Se_8$.

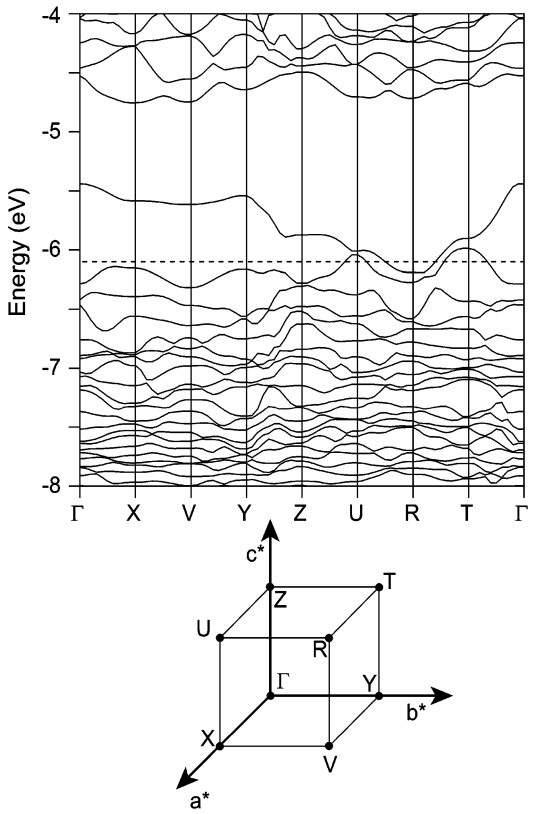

Figure 7. Band structure of $Cu_4Mo_6Se_8$ calculated using DFT. The dotted line represents the Fermi level. The location of the special *k* points used in the band-structure plot are also shown.

Electronic Structure. The band structure of $Cu_4Mo_6Se_8$, calculated using plane-wave DFT is shown in Figure 7. The calculations show this compound to be a semimetal, with a single band dipping below the Fermi level at *R*. Figure 8 shows the corresponding density of states and projected densities of states. This figure shows that the band just above the Fermi level is derived primarily from Mo orbitals, with some Se and Cu contributions. We find that, near the Fermi level, there is good agreement between the DFT results shown in Figure 7 and the band structure calculated at the extended Hückel level. Thus, we proceed to analyze the electronic structure of this compound using extended Hückel methods, paying particular attention to the band that lies between about −6 and −5.5 eV in Figure 7.

We begin by examining the molecular orbitals of an ideal Mo_6Se_8 cluster, that is, a perfect cube of Se atoms with Mo atoms at the centers of the six faces. A careful study of this model for the sulfide cluster, as well as the effect of crystallizing these clusters in the Chevrel phase motif, has been presented by Hughbanks and Hoffmann.[10] They find that the frontier orbitals are all primarily Mo 4d in character. Upon crystallization, the faces of the cube are capped by chalcogens on neighboring clusters, which pushes a set of five unoccupied orbitals up in energy, These orbitals all have large lobes directed out of the cube faces toward the capping sulfur atoms. The increase in energy of these orbitals produces a large HOMO−LUMO gap for the cluster of

(41) *Current Topics in Materials Science vol. 3*; Kaldis, E., Ed.; Elsevier: Amsterdam, 1979.
(42) Bars, O.; Guillevic, J.; Grandjean, D. *J. Solid State Chem.* **1973**, *6*, 48.
(43) Zabrodsky, H.; Peleg, S.; Avnir, D. *J. Am. Chem. Soc.* **1992**, *114*, 7843. Pinsky, M.; Avnir, D. *Inorg. Chem.* **1998**, *37*, 5575.
(44) *SHAPE v1.1a_02, Continuous Shape Measures calculation*, 2003.

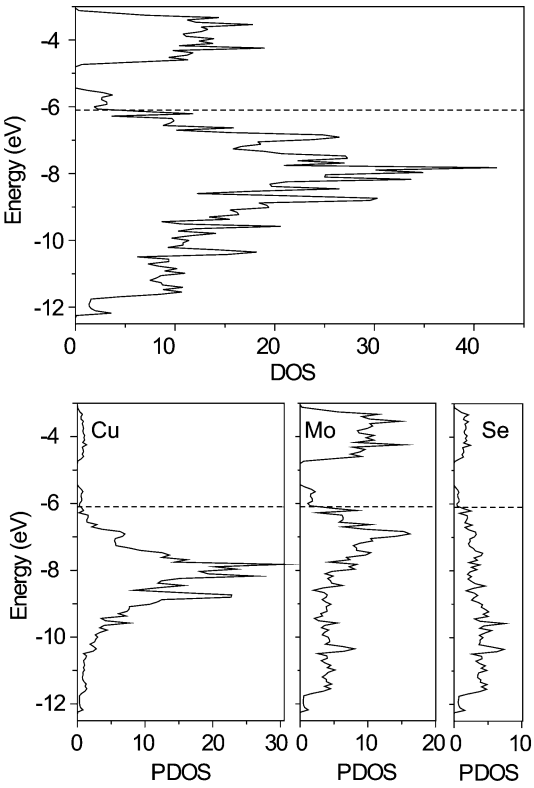

Figure 8. Calculated total density of states (DOS) and partial densities of states (PDOS) for $Cu_4Mo_6Se_8$ calculated with DFT.

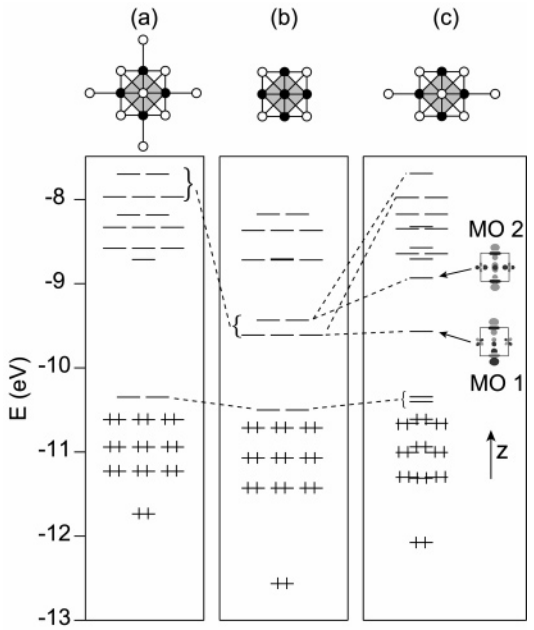

Figure 9. Extended Hückel molecular orbital diagrams for (a) an Mo_6Se_8 cluster with six capping Se atoms as found in classic Chevrel phases, (b) a bare Mo_6Se_8 cluster, and (c) an Mo_6Se_8 cluster with four equatorial Se ligands, as found in $Cu_4Mo_6Se_8$.

charge −4. This is the molecular origin of the energy gap seen in the semiconducting Chevrel phases.

We show results from a similar calculation for the neutral selenide cluster in Figure 9. In this figure, panel b shows molecular orbitals for the uncapped Mo_6Se_8 cluster while panel a shows the results of capping each face with Se. These MO diagrams are very similar to those calculated for the sulfide cluster.[10] Panel c in Figure 9 shows the result of capping only four of the six faces of the cubic cluster. This approximates the situation found in $Cu_4Mo_6Se_8$. In this case, we see that two of the five energy levels are "left behind". These correspond to orbitals directed primarily out of the uncapped faces. Representations of these orbitals, labeled MO 1 and MO 2, are also shown in Figure 9c. We will see that it is MO 1 which evolves into the band of interest in the 3-D structure.

Figure 10 shows how the band structure of the 3-D structure evolves from the MO diagram shown in Figure 9c. For ease of comparison, this MO diagram is reproduced in panel a of Figure 10. Panel b shows the bands for a single sheet of composition Mo_6Se_8, extracted from the structure of $Cu_4Mo_6Se_8$. As expected, band 1 and band 2, which originate from MO 1 and MO 2, respectively, show little dispersion since these MOs are primarily directed perpendicular to the sheet.

Figure 10c shows the calculated band structure for a stack of such sheets, such as that which occurs in $Cu_4Mo_6Se_8$. Here significant band dispersion is observed in band 1 and band 2, especially in directions perpendicular to the sheets. We see that band 1 runs down from Γ to Z, while band 2 runs up. This is consistent with the reflection symmetry of MO 2 (mirror plane perpendicular to the *z* direction) and the reflection antisymmetry of MO 1 (Figure 9). We note here that the apparent degeneracy of these two bands at Γ is accidental.

Finally, Figure 10d shows the extended Hückel band structure for the full $Cu_4Mo_6Se_8$ structure. We first note the striking similarities to the band structure calculated using DFT (see Figure 7), especially near the Fermi level. The only difference between the crystal structures in Figure 10c and d is the Cu atoms which are included in panel d but not in panel c. Figure 10c shows that, in the rigid-band approximation, the four electrons donated to the Mo_6Se_8 framework by four Cu^{1+} ions would produce a semiconducting compound, filling the two empty bands below band 1. However, since the Cu atoms in $Cu_4Mo_6Se_8$ are situated between the uncapped cluster faces, they interact with bands 1 and 2. This interaction lowers the energy of band 1 so that it dips below the Fermi level, making $Cu_4Mo_6Se_8$ a semimetal, not a semiconductor.

Magnetic Susceptibility. Since many metallic phases with the classical Chevrel phase structure are superconducting, magnetic susceptibility measurements were performed between 4 and 20 K on a powder sample containing a mixture of approximately equal amounts of $Cu_{\sim 2}Mo_6Se_8$ and $Cu_4Mo_6Se_8$. The measurements showed only a single superconducting transition near 6 K. This is close to the previously measured T_C for $Cu_2Mo_6Se_8$ of 5.9 K.[2] At 4 K, the diamagnetic susceptibility had not yet saturated, and its value suggests that only a small volume fraction (∼2%) of the sample was superconducting. These observations suggest that $Cu_4Mo_6Se_8$ is not a superconductor above 4 K.

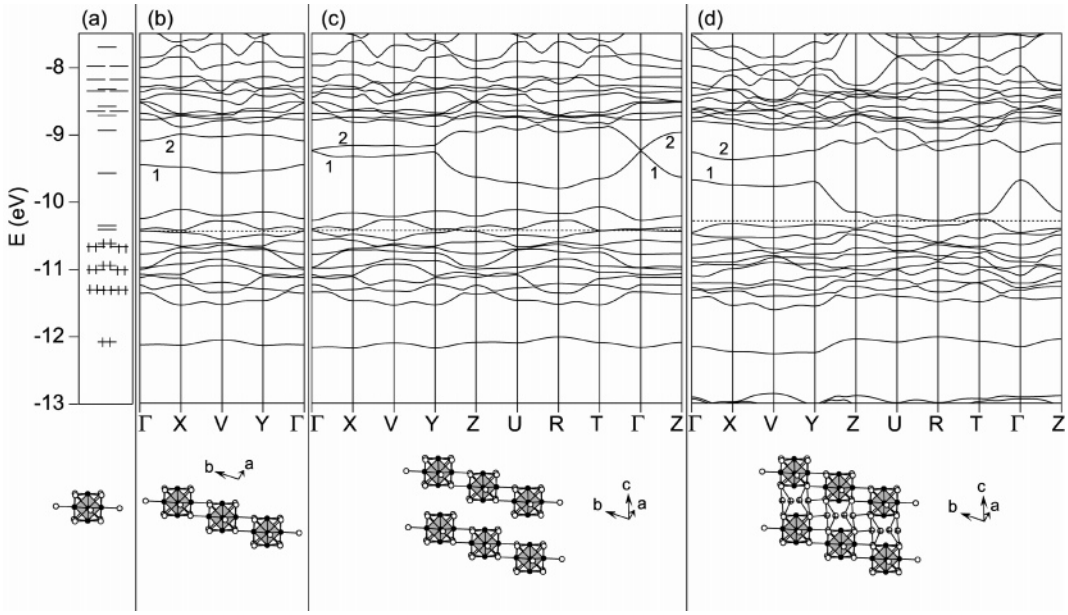

Figure 10. Evolution of the band structure of $Cu_4Mo_6Se_8$ from (a) molecular orbitals, to (b) two-dimensional sheets, to (c) stacked sheets, to (d) the full $Cu_4Mo_6Se_8$ structure.

Conclusions

In this work, we have demonstrated an alternative method for intercalating Cu into Chevrel phase materials ($Cu_xMo_6Q_8$, Q = S, Se, Te) at room temperature. This method produced maximum Cu contents in agreement with those reported for high-temperature syntheses for the sulfides ($x = 3.7$) and selenides ($x = 3.0$). The success of this and other intercalation methods is dependent upon the relatively high mobility of Cu ions in the Chevrel phase structure. This ionic conduction may limit the use of Cu-filled Chevrel phases for high-temperature thermoelectric power generators.

These studies also led to the identification of the new Chevrel phase polymorph $Cu_4Mo_6Se_8$, which had been previously observed only as unidentified reflections in powder diffraction studies.[13] We have reported here the structure of this phase, determined by single-crystal X-ray diffraction. This structure represents the first example of extended Mo_6Se_8 sheets which are not connected to one another through Mo−Se bonding. The location of the Cu atoms, between faces of Mo_6Se_8 clusters in neighboring sheets, separates the layers along the *c* axis. The only connections between the layers are through Cu−Se interactions.

The separation of the Mo_6Se_8 layers and the location of the Cu atoms have interesting electronic consequences. Although $Cu_4Mo_6Se_8$ has formally 24 electrons per metal cluster, and therefore should be a semiconductor according to the usual electron counting schemes, band-structure calculations predict this material to be metallic. Analysis of extended Hückel calculations show this to be due to the interaction between the Cu atoms and Mo-based molecular orbital pointed toward the "missing" Se.

Acknowledgment. This work was funded by NASA/JPL. We are grateful to Anneliese M. Schmidt for help with some of the high-temperature Chevrel phase synthesis and Franck Gascoin and G. Jeffrey Snyder for informative discussions and interactions. We also thank Dr. Emil B. Lobkovsky for assistance in collecting single-crystal X-ray diffraction data and John Hunt for guidance in using the electron microprobe facility in the Cornell Center for Materials Research which is supported through a MRSEC Grant (DMR-0520404).

Supporting Information Available: Crystallographic information in the form of a cif file. This material is available free of charge via the Internet at http://pubs.acs.org.

IC052013P